Solid State Ionics 180 (2009) 812–816

Contents lists available at ScienceDirect

Solid State Ionics

journal homepage: www.elsevier.com/locate/ssi

Oxygen transport in $La_2NiO_{4+\delta}$: Assessment of surface limitations and multilayer membrane architectures

A.L. Shaula [a,b,*], E.N. Naumovich [a], A.P. Viskup [c], V.V. Pankov [c], A.V. Kovalevsky [a,d], V.V. Kharton [a]

[a] Department of Ceramics and Glass Engineering, CICECO, University of Aveiro, 3810-193 Aveiro, Portugal
[b] Department of Mechanical Engineering, SEG-CEMUC, University of Coimbra, Polo II, 3030-788 Coimbra, Portugal
[c] Institute for Physicochemical Problems, Belarus State University, 14 Leningradskaya Str., 220050 Minsk, Belarus
[d] Materials Department, Flemish Institute for Technological Research (VITO), 2400 Mol, Belgium

ARTICLE INFO

Article history:
Received 15 September 2008
Received in revised form 6 January 2009
Accepted 8 January 2009

Keywords:
Lanthanum nickelate
Oxygen permeability
Oxygen exchange kinetics
Phenomenological modelling
Surface modification
Multilayer architecture
Tape casting

ABSTRACT

The steady-state oxygen permeation through dense $La_2NiO_{4+\delta}$ ceramics, limited by both surface exchange and bulk ambipolar conduction, can be increased by deposition of porous layers onto the membrane surfaces. This makes it possible, in particular, to analyze the interfacial exchange kinetics by numerical modelling using experimental data on the oxygen fluxes and equilibrium relationships between the oxygen chemical potential, nonstoichiometry and total conductivity. The simulations showed that the role of exchange limitations increases on reducing oxygen pressure, and becomes critical at relatively large chemical potential gradients important for practical applications. The calculated oxygen diffusion coefficients in $La_2NiO_{4+\delta}$ are in a good agreement with literature. In order to enhance membrane performance, the multilayer ceramics with different architecture combining dense and porous components were prepared via tape-casting and tested. The maximum oxygen fluxes were observed in the case when one dense layer, ~60 μm in thickness, is sandwiched between relatively thin (<150 μm) porous layers. Whilst the permeability of such membranes is still affected by surface-exchange kinetics, increasing thickness of the porous supporting components leads to gas diffusion limitations.

1. Introduction

Mixed-conducting materials derived from K_2NiF_4-type $La_2NiO_{4+\delta}$ are of substantial interest for high-temperature electrochemical applications, in particular, cathodes of solid oxide fuel cells (SOFCs) and ceramic membranes for oxygen separation and natural gas conversion reactors [1–11]. The advantages of La_2NiO_4-based compositions include relatively high oxygen ionic and p-type electronic conductivities, moderate thermal and chemical expansion, and high electrocatalytic activity. The oxygen permeability of dense nickelate membranes is essentially limited by kinetics of surface redox processes [1,3,6,10], which prevents bulk decomposition and enables stable operation under air/CH_4 gradients up to temperatures as high as 1173 K [4]. At the same time, partial reduction of the nickelate surface exposed to reducing atmosphere results in the formation of porous La_2O_3-supported Ni catalyst layer, providing a high selectivity towards partial oxidation of methane [5]. One promising concept for the ceramic membrane developments relates to asymmetric configurations where a thin dense highly-permeable layer is sandwiched between two porous sheets made of similar compositions [12–14]. The porous components enhance specific surface area and exchange rates, and may simultaneously act as the membrane and catalyst supports and, when necessary, protective diffusion barriers preventing surface poisoning and reductive decomposition. The present work was focused on the evaluation of surface contributions to the oxygen chemical potential drop across $La_2NiO_{4+\delta}$ membranes, and on the assessment of multilayer nickelate ceramics with porous layers, prepared using tape-casting.

2. Experimental

The powder of $La_2NiO_{4+\delta}$ was synthesized by glycine-nitrate process (GNP), followed by annealing in air at 1070–1370 K for 2–4 h and subsequent ball-milling. X-ray diffraction (XRD) analysis confirmed the formation of single K_2NiF_4-type phase (space group *I4/mmm*, unit cell parameters: $a = 3.8646(4)$ Å, $c = 12.691(4)$ Å). The disk-shaped samples, hereafter referred to as "standard", were uniaxially pressed at 150–200 MPa and sintered at 1590 ± 5 K for 2 h in air. The density of the standard $La_2NiO_{4+\delta}$ membranes was $98 \pm 1\%$ of their theoretical density calculated from XRD data; the thickness (L) varied in the range 0.6–1.0 mm. For the fabrication of multilayer ceramics via tape-casting, slurries containing the as-prepared $La_2NiO_{4+\delta}$ powder without or with

* Corresponding author. Department of Mechanical Engineering, SEG-CEMUC, University of Coimbra, Polo II, 3030-788 Coimbra, Portugal.
E-mail address: ashaula@cv.ua.pt (A.L. Shaula).

0167-2738/$ – see front matter © 2009 Elsevier B.V. All rights reserved.
doi:10.1016/j.ssi.2009.01.005

graphite pore-forming additive (3 wt.%), ethanol, butyl acetate, butyral resin and a plasticizer were introduced in an injection-molding machine and a series of 30 ± 1 μm thick tapes were fabricated; then the membranes with different architecture were prepared by laminating various sets of these tapes and sintering at 1570 ± 5 K for 2 h. In this work, data on four types of the tape-casted membranes are compared. The first two are based on single-layer dense ceramics with $L = 0.35$ mm without or with feed-side surface modification. In the latter case, porous layers of $La_2NiO_{4+\delta}$ (sheet density of 2–4 mg/cm^2) were deposited onto the feed side surface of the sintered single-layer ceramics. Hereafter these membranes are denoted as "1-layer" and "1-layer activated", respectively. Fig. 1A illustrates the morphology of porous activating layer, evaluated by scanning electron microscopy (SEM). The 3-layer membranes of another group comprised a dense layer with $L \approx 60$ μm and two porous layers, 50 and 140 μm, as displayed by Fig. 1B. Similar membranes with thicker porous components were obtained sandwiching the as-laminated 3-layer compact between two additional layers made of $La_2NiO_{4+\delta}$ powder, graphite (15 wt.%) and polyvinyl acetate (3–5 wt.%). The resultant microstructure of the sintered 5-layer ceramics, tested in order to assess impact of the relatively thick membrane/catalyst supports, is shown in Fig. 1C. In selected cases, the porous supports were additionally modified infiltrating a very small amount of praseodymium oxide, known for its high catalytic activity in electrochemical reactions involving molecular oxygen [6,12], into the pores by impregnation with a diluted $Pr(NO_3)_3$ solution in ethanol and subsequent thermal decomposition at 800–900 K. The equipment and procedures used for microstructural characterization, oxygen permeation tests, total conductivity measurements and numerical modelling, were described elsewhere (see Refs. [3,4,6,15–17] and references cited). All data on steady-state oxygen permeability presented in this work correspond to the feed-side oxygen partial pressure, $p(O_2)_{feed}$, equal to atmospheric; the permeate-side oxygen pressure, $p(O_2)_{perm}$, varied in the range 5×10^{-3} to 0.2 atm. The reproducibility error of the oxygen permeation fluxes through dense $La_2NiO_{4+\delta}$ membranes was less than 10–12%; in the case of multilayer ceramics where the permeability is strongly affected by minor microstructural differences and defects in the porous supports, this error achieved 25–30%.

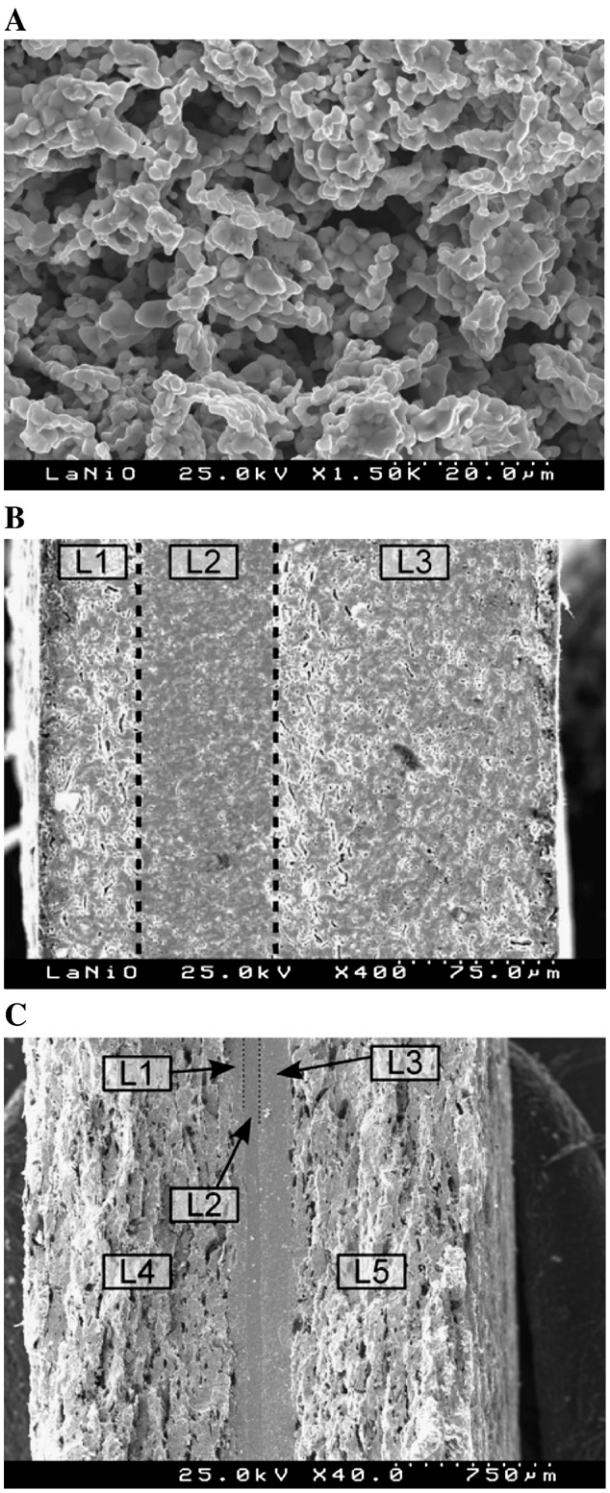

Fig. 1. SEM micrographs of the activated feed-side surface of monolayer $La_2NiO_{4+\delta}$ membrane (A), and cross-sections of 3-layer (B) and 5-layer (C) ceramics. For (B) and (C), L2 corresponds to the dense central layer; L1 and L3 are thin porous layers. L4 and L5 in (C) correspond to the additional porous layers.

3. Results and discussion

Fig. 2 compares the oxygen permeation fluxes (j) through mono- and multilayer $La_2NiO_{4+\delta}$ membranes, shown as a function of the oxygen pressure gradient at 1123 and 1223 K. The deposition of porous layers leads to a substantially higher permeation, thus confirming that the overall oxygen transport is affected by surface exchange kinetics, in agreement with literature data revealing that the role of interfacial exchange as a permeation-limiting factor increases when temperature or oxygen partial pressure decreases [1,3,6,10]. A similar conclusion on non-negligible impact of the surface processes can be drawn analyzing the membrane thickness dependence of oxygen fluxes through the standard $La_2NiO_{4+\delta}$ ceramics without surface activation (Fig. 3). Note also that reducing permeate-side oxygen pressure leads to a smaller difference between the membranes with different thicknesses. Another necessary comment is that the effect of surface modification on the permeability of monolayer tape-casted membranes with $L = 0.35$ cm is almost invisible, comparable to the experimental error at 1223 K, but becomes obvious at 1123 K (Fig. 2).

This behavior makes it possible to model all rate-determining steps of the oxygen transport process by splitting the overall oxygen chemical potential gradient across $La_2NiO_{4+\delta}$ membranes into three parts, which correspond to the membrane bulk ($\Delta\mu_{bulk}$) and to the permeate-side ($\Delta\mu_{perm}$) and feed-side ($\Delta\mu_{feed}$) surfaces. The bulk contribution is determined by the partial ionic and electronic conductivities according to the Wagner equation:

$$j = \frac{1}{16F^2L}\int_{\mu^s_{perm}}^{\mu^s_{feed}} \sigma_{amb}\, d\mu = \frac{RT}{16F^2L}\int_{\mu^s_{perm}}^{\mu^s_{feed}} \sigma_O\left(1 - \frac{\sigma_O}{\sigma}\right) d\mu \qquad (1)$$

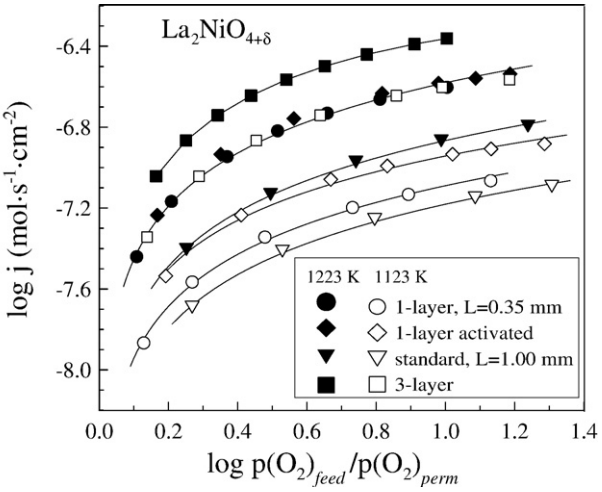

Fig. 2. Comparison of the oxygen permeation fluxes through mono- and multilayer $La_2NiO_{4+\delta}$ membranes at 1123 and 1223 K. The solid lines are for visual guidance only.

where μ is the oxygen chemical potential, and μ^s_{feed} and μ^s_{perm} are the μ values at the feed- and permeate-side surfaces, correspondingly. In this equation, σ, σ_{amb} and σ_O are the total, ambipolar and partial oxygen-ionic conductivities, respectively. For numerical modeling, experimental data on the total conductivity of $La_2NiO_{4+\delta}$ (Fig. 4A) collected in this work were used. Taking into account that ion diffusion in lanthanum nickelate occurs predominantly via the interstitial migration mechanism and that the concentration of hyperstoichiometric oxygen anions ([O"] or δ) under ambient conditions is significantly lower with respect to the number of available interstitial positions [1–3,7–10,17], the oxygen ionic conductivity was defined as

$$\sigma_o = K_o[O'']\tag{2}$$

where K_O is a temperature-dependent constant proportional to the oxygen diffusion coefficient. The relationships between oxygen chemical potential, interstitial concentration and temperature were reported in previous work [17]. The oxygen transfer through membrane/gas interfaces was expressed using a classical non-equilibrium thermodynamic expression [18]:

$$j = J^0 \cdot \left(1 - \exp\left[\frac{\Delta\mu_i}{n_{lim}RT}\right]\right)\tag{3}$$

where J^0 is the equilibrium exchange rate, and n_{lim} is the stoichiometric coefficient showing the ratio between the fluxes of molecular O_2 and species involved in the rate-determining step of the interfacial exchange process. Eq. (3) represents a simplified solution of the model [19] proposed for oxygen exchange between a mixed ionic-electronic conductor and gas phase, and is qualitatively similar to the equation for solid-electrolyte cells where increasing electrode polarization leads to limiting currents [20]. In the latter case, physical meaning of J^0 relates to the limiting flux of electrochemically active species, which may be governed by diffusion, adsorption or chemical reaction steps [20].

In the course of numerical calculations using this approach (Model 1), the independent variables (X_i) included oxygen chemical potential in the gaseous phase over the membrane feed side (μ^{gas}_{feed}), j and L, whilst the chemical potential over permeate-side surface (μ^{gas}_{perm}) was treated as dependent variable (Y). The integral term in Eq. (1) was interpolated by Chebyshev series and than solved analytically [21]; the calculations were performed utilizing appropriate functions from the GNU scientific library [22]. The regression

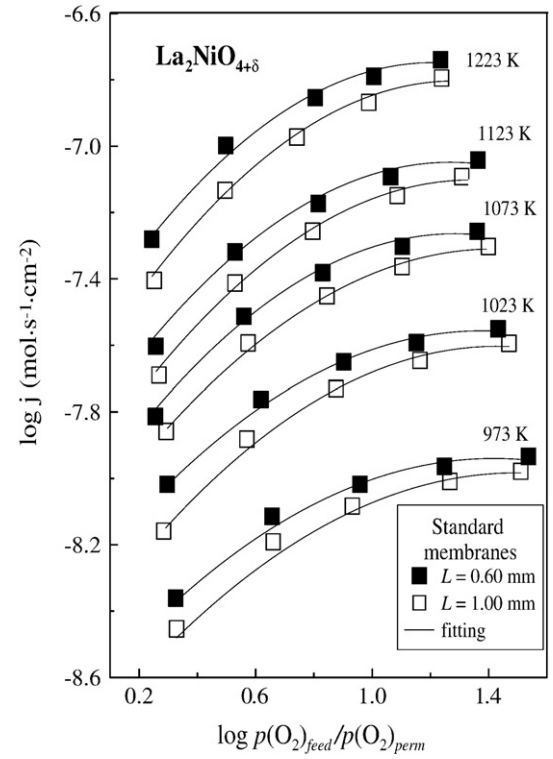

Fig. 3. Oxygen permeation fluxes through standard $La_2NiO_{4+\delta}$ membranes without surface modification. Solid lines correspond to the fitting results using Model 1.

parameters included J^0 and K_O (Table 1). The best fitting quality was obtained by fixing the n_{lim} value equal to 2. Introducing n_{lim} as a regression parameter caused statistical degeneration of the model; considering other possible values having definite physical meaning also led to considerably higher errors. As an example, Table 1 compares the regression parameters obtained by fixing $n_{lim} = 1$, 2 and 4.

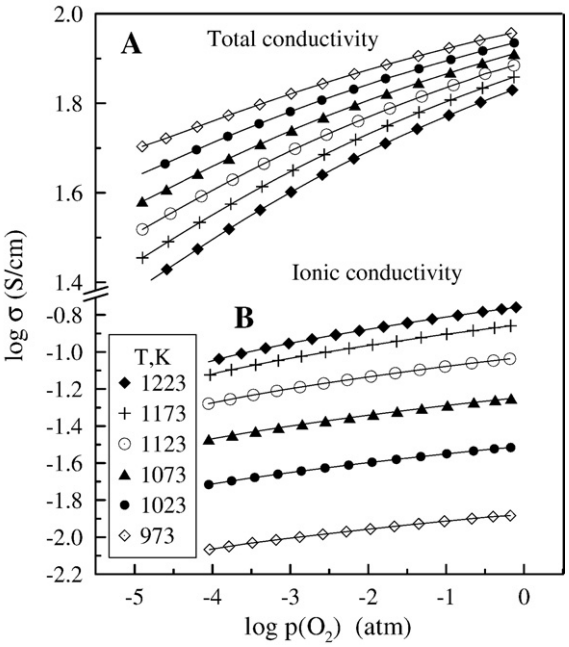

Fig. 4. Oxygen partial pressure dependencies of the total (A) and oxygen ionic (B) conductivities of $La_2NiO_{4+\delta}$. The ionic conductivity was calculated numerically from the oxygen permeation, nonstoichiometry and total conductivity data using Model 1 (see text).

Table 1
Regression parameters for the oxygen permeation fluxes through standard $La_2NiO_{4+\delta}$ membranes using Model 1.

T, K	K_O, S/cm	J^0, nmol/(s×cm^2)	n_{lim}	R_{adj}*
1223	1.92 ± 0.08	220 ± 3	2	0.9994
1173	1.5 ± 0.1	152 ± 2		0.9997
1123	0.96 ± 0.06	104 ± 2		0.9990
1073	0.56 ± 0.02	63.7 ± 0.8		0.9995
1023	0.29 ± 0.01	31.5 ± 0.4		0.9991
973	0.12 ± 0.01	12.9 ± 0.4		0.996
1223	1.4 ± 0.1	200 ± 20	4	0.990
1223	2.5 ± 0.4	300 ± 20	1	0.997

* R_{adj} is the adjusted correlation coefficient.

The best fitting results, with $n_{lim}=2$, are shown in Fig. 3 as solid lines.

The calculated ionic conductivity (Fig. 4B) was combined with equilibrium oxygen nonstoichiometry [17] in order to assess the oxygen self-diffusion coefficients by the Nernst–Einstein equation [12]. The results displayed in Fig. 5 are in a reasonable agreement with literature data on $La_2NiO_{4+\delta}$ ceramics [2,10].

Extrapolation of the simulation results towards lower oxygen chemical potentials (Fig. 6) shows that, due to increasing surface limitations, the oxygen fluxes tend to become thickness-independent when the chemical potential gradient increases. These "limiting-flux" regimes are observed under conditions close to the perspective operation mode where $La_2NiO_{4+\delta}$ membranes are used for oxygen enrichment of carbon dioxide supplied then in a hydrocarbon conversion reactor [1]. For the potential practical applications, this tendency makes it necessary to enhance surface-exchange kinetics by increasing specific surface area of the nickelate membranes and/or by incorporating highly-active exchange catalysts with nano-scale particle size into the pores. At the same time, the appearance of limiting fluxes (J^0_{lim}) enables to describe the oxygen transport rate by a simplified equation, referred to as Model 2:

$$j = J^0_{lim}\left(1 - \sqrt{\frac{p(O_2)_{perm}}{p(O_2)_{feed}}}\right) \quad (4)$$

As illustrated by Fig. 7, Model 2 is quite adequate for $La_2NiO_{4+\delta}$ membranes placed under moderate oxygen pressure gradients. At relatively low oxygen pressures, however, Model 2 predicts an asymptotic rise of oxygen fluxes, which contradicts to the experimental observations. This approximative equation can therefore be used for oxidizing conditions only.

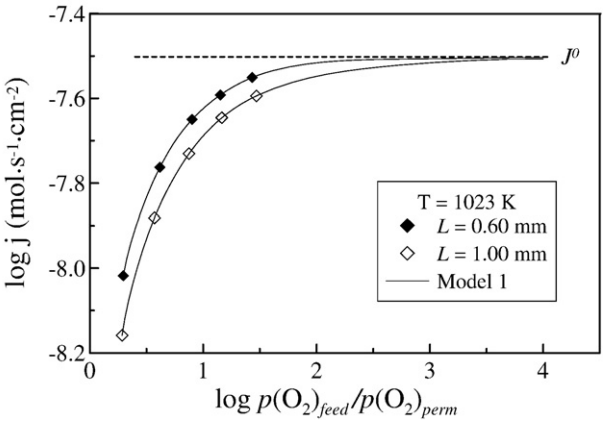

Fig. 6. Oxygen permeation fluxes through standard $La_2NiO_{4+\delta}$ membranes, extrapolated to large $p(O_2)$ gradients using the regression parameters of Model 1.

For the membranes studied in this work, maximum oxygen permeation was observed for the tape-casted 3-layer ceramics, where the effective area of both membrane surfaces is enlarged by porous layers and the thickness of all components is moderate (Figs. 2 and 8). The corresponding oxygen fluxes are 3–5 times higher compared to the standard $La_2NiO_{4+\delta}$ ceramics with $L=1.0$ mm. On the other hand, however, these fluxes are still much lower than theoretical, expected for zero surface limitations. As an example, at $p(O_2)_{feed}=0.21$ atm and $p(O_2)_{perm}=0.021$ atm, theoretical values of the bulk diffusion-limited oxygen fluxes through the 3-layer membrane are approximately 2 times higher with respect to the experimental data at 1273 K; on cooling down to 973 K, their difference becomes greater than 3 times.

The same conclusion can be drawn from the fact that the apparent activation energy for oxygen transport in the 3-layer membranes at 973–1223 K is similar to that observed for the thick standard ceramics (Fig. 8). Applying additional porous layers onto the membrane surfaces in the 5-layer design decreases oxygen permeation and its activation energy, thus unambiguously indicating an increased role of oxygen gas diffusion in the pores. This effect is considerably larger compared to the level of experimental uncertainties, despite the relatively high errors typical for the multilayer membranes as

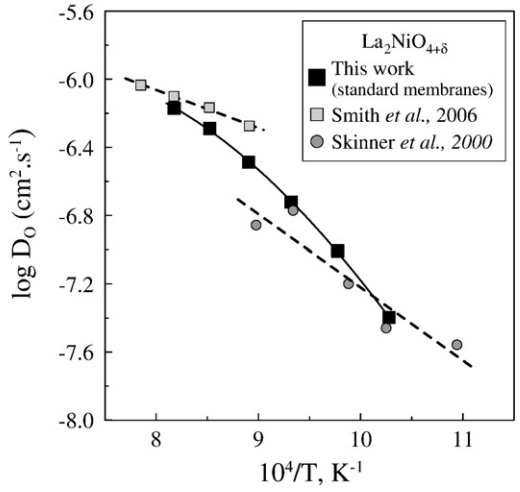

Fig. 5. Comparison of the calculated self-diffusion coefficients of oxygen anions in $La_2NiO_{4+\delta}$ and literature data [2,10].

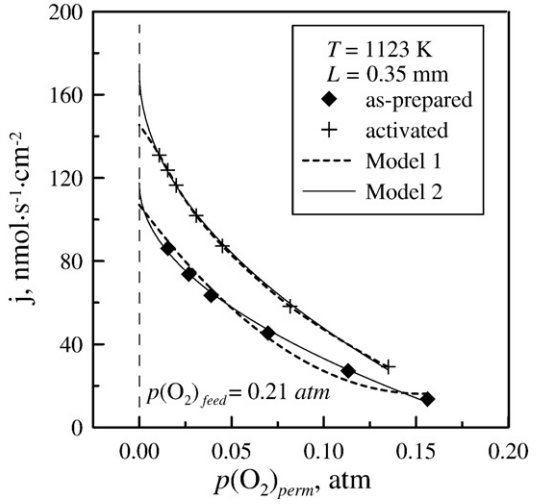

Fig. 7. Comparison of the fitting results using Models 1 and 2, for the tape-casted 1-layer membranes with and without surface modification.

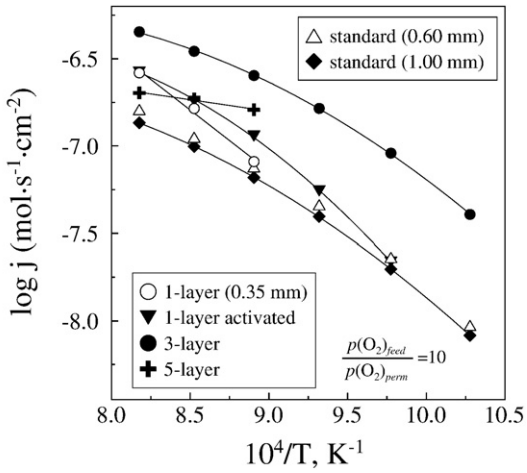

Fig. 8. Temperature dependencies of the oxygen permeation fluxes through $La_2NiO_{4+\delta}$ membranes under fixed $p(O_2)$ gradient.

mentioned above. The infiltration of praseodymium oxide into the pores was found to have a weak negative impact on the oxygen permeability, confirming that the overall porosity and pore size of the supports play a more important role with respect to the electrocatalytic activity. Although the gas diffusion limitations can be partly suppressed via thorough microstructural optimization of the porosity-graded supports, this factor requires to reduce thickness of the porous layers down to 100–200 μm, as for the SOFC electrodes; modelling of the interfacial phenomena in the multilayer membranes should account for molecular oxygen diffusion in the gaseous phase.

4. Conclusions

The steady-state oxygen permeation through $La_2NiO_{4+\delta}$ ceramics is governed by both interfacial exchange kinetics and bulk ambipolar conductivity, and can be increased via surface modification. In this work a series of lanthanum nickelate membranes with various architectures, prepared using glicine-nitrate process and tape-casting, were examined. The maximum oxygen transport was observed for the membranes where when one dense layer (~60 μm in thickness) is sandwiched between relatively thin (<150 μm) porous layers. Increasing thickness of the porous supporting components and infiltration of catalytically active praseodymium oxide into the pores were found to decrease the permeability due to gas diffusion limitations. The interfacial exchange kinetics was analyzed by numerical modelling using experimental data on the oxygen fluxes and equilibrium relationships between the oxygen chemical potential, oxygen nonstoichiometry and total conductivity. The calculated ion diffusion coefficients in $La_2NiO_{4+\delta}$ are close to the literature data. The surface exchange limitations increase on reducing oxygen pressure and become critical at relatively large chemical potential gradients important for practical applications.

Acknowledgements

This work was supported by the FCT, Portugal (projects PTDC/CTM/64357/2006, POCI/CTM/ 59197/2004 and SFRH/BPD/28913/2006), by the Belgian Federal Science Policy foundation, and by the Belarus Ministry of Education.

References

[1] B. Vigeland, R. Glenne, T. Breivik and S. Julsrud, Int. Patent Application PCT WO 99/59702 (1999).
[2] S.J. Skinner, J.A. Kilner, Solid State Ionics 135 (2000) 709.
[3] V.V. Kharton, A.P. Viskup, E.N. Naumovich, F.M.B. Marques, J. Mater. Chem. 9 (1999) 2623.
[4] V.V. Kharton, A.A. Yaremchenko, A.A. Valente, V.A. Sobyanin, V.D. Belyaev, G.L. Semin, S.A. Veniaminov, E.V. Tsipis, A.L. Shaula, J.R. Frade, J. Rocha, Solid State Ionics 176 (2005) 781.
[5] D.C. Zhu, X.Y. Xu, S.J. Feng, W. Liu, C.S. Chen, Catal. Today 82 (2003) 151.
[6] V.V. Kharton, E.V. Tsipis, A.A. Yaremchenko, J.R. Frade, Solid State Ionics 166 (2004) 327.
[7] E. Boehm, J.M. Bassat, M.C. Steil, P. Dordor, F. Mauvy, J.C. Grenier, Solid State Sci. 5 (2003) 973.
[8] M. Al Daroukh, V.V. Vashook, H. Ullmann, F. Tietz, I. Arual Raj, Solid State Ionics 158 (2003) 141.
[9] A. Aguadero, J.A. Alonso, M.J. Martinez-Lope, M.T. Fernandez-Diaz, M.J. Escudero, L. Daza, J. Mater. Chem. 16 (2006) 3402.
[10] J.B. Smith, T. Norby, J. Electrochem. Soc. 153 (2006) A233.
[11] V.V. Kharton, A.V. Kovalevsky, M. Avdeev, E.V. Tsipis, M.V. Patrakeev, A.A. Yaremchenko, E.N. Naumovich, J.R. Frade, Chem. Mater. 19 (2007) 2027.
[12] H.J.M. Bouwmeester, A.J. Burggraaf, in: A.J. Burggraaf, L. Cot (Eds.), Fundamentals of Inorganic Membrane Science and Technology, Elsevier Science, Amsterdam, 1996, p. 435.
[13] M.F. Carolan, P.N. Dyer, US Patent 5534471 (1996).
[14] G. Etchegoyen, T. Chartier, P. Del-Gallo, J. Eur. Ceram. Soc. 26 (2006) 2807.
[15] M.V. Patrakeev, E.B. Mitberg, A.A. Lakhtin, I.A. Leonidov, V.L. Kozhevnikov, V.V. Kharton, M. Avdeev, F.M.B. Marques, J. Solid State Chem. 167 (2002) 203.
[16] E.V. Tsipis, E.N. Naumovich, A.L. Shaula, M.V. Patrakeev, J.C. Waerenborgh, V.V. Kharton, Solid State Ionics 179 (2008) 57.
[17] E.N. Naumovich, M.V. Patrakeev, V.V. Kharton, A.A. Yaremchenko, D.I. Logvinovich, F.M.B. Marques, Solid State Sci. 7 (2005) 1353.
[18] S.R. de Groot, P. Mazur, Nonequilibrium Thermodynamics, Dover, New York, 1984.
[19] S.B. Adler, X.Y. Chen, J.R. Wilson, J. Catal. 245 (2007) 91.
[20] V.N. Chebotin, M.V. Perfiliev, Electrochemistry of Solid Electrolytes, Technical Information Center, US Department of Energy, Oak Ridge, 1978.
[21] M. Abramowitz, I. Stegun (Eds.), Handbook of Mathematical Functions with Formulas, Graphs, and Mathematical Tables, Dover Publ., New York, 1972.
[22] http://www.gnu.org/software/gsl/.